

Article

Enhancement of γ/γ' Microstructured Cobalt Superalloys Produced from Atomized Powder by Creating a Harmonic Structure

Mónica Campos ¹, Marta Cartón-Cordero ², Lucía García de la Cruz ¹, Francisca G. Caballero ², Jonathan D. Poplawsky ³ and José M. Torralba ^{1,4,*}

- ¹ Powder Tech. Group, Department of Materials Science and Engineering, Universidad Carlos III Madrid, 28911 Leganés, Spain; campos@ing.uc3m.es (M.C.); lgcruz@ing.uc3m.es (L.G.d.l.C.)
- ² Department of Physical Metallurgy, National Center for Metallurgical Research (CENIM-CSIC), Avda. Gregorio del Amo, 8. E-28040 Madrid, Spain; fgc@cenim.csic.es (F.G.C.)
- ³ Center for Nanophase Materials Sciences, Oak Ridge National Laboratory, Oak Ridge, TN 37830, USA; poplawskyjd@ornl.gov
- ⁴ IMDEA Materials Institute, 28906 Getafe, Spain
- * Correspondence: torralba@ing.uc3m.es

Abstract: A material's properties must be continuously improved to meet the demands of extreme conditions in high-temperature applications. It is demonstrated that γ - γ' Co-based superalloys could surpass the yield stress of Ni-based superalloys at high temperature due to the γ - γ' structure. The powders were subjected to a harmonic modification in order to refine the grain structure on the surface and to activate the sintering process. This study examines how harmonic structure affects microstructure and mechanical properties at high temperatures. Spark Plasma Sintering (SPS) was used for consolidation to maintain the ultrafine grain size microstructure of the powder. Compression tests were conducted from room temperature (RT) to 750 °C to assess the mechanical properties of the material. Yield stress values obtained from harmonic structures are four times higher than those obtained from cast alloys.

Keywords: co-based superalloys; γ - γ' strengthening; harmonic structure



Citation: Campos, M.; Cartón-Cordero, M.; García de la Cruz, L.; Caballero, F.G.; Poplawsky, J.D.; Torralba, J.M. Enhancement of γ/γ' Microstructured Cobalt Superalloys Produced from Atomized Powder by Creating a Harmonic Structure. *Metals* **2024**, *14*, 70. <https://doi.org/10.3390/met14010070>

Academic Editors: Maciej Motyka and Wei Liu

Received: 2 December 2023

Revised: 19 December 2023

Accepted: 5 January 2024

Published: 7 January 2024



Copyright: © 2024 by the authors. Licensee MDPI, Basel, Switzerland. This article is an open access article distributed under the terms and conditions of the Creative Commons Attribution (CC BY) license (<https://creativecommons.org/licenses/by/4.0/>).

1. Introduction

In 2006, Sato et al. [1] found the presence of an L12 structure in the Co-Al-W ternary diagram at 900 °C and 1000 °C, of precipitates with $\text{Co}_3(\text{Al}, \text{W})$ stoichiometry, presenting a cubic structure coherent with the fcc-matrix. From that point on, those precipitates were denominated γ' . Suzuki et al. [2] measured the yield stress of this new family of Co-based superalloys at high temperature with a behavior similar to some commercial Ni-based superalloys. Even higher values of yield strength were obtained when 2% of Ta, a γ' stabilizer, was added to the Co-9Al-10W (at.%). These findings opened a new path to develop new Co-based superalloys with similar mechanical behavior as Ni-based superalloys. The similarities between Ni and Co suggest that some strategies used for the development of Ni-based superalloys could be used in the new Co-based superalloys. However, the area of stability of the γ' precipitates in the Co-Al-W ternary diagram is smaller at high temperatures, compared to γ' precipitates in Ni-based superalloys [1,3]. To increase the stability area of the L12 phase in Co-based superalloys, a study was conducted using parallel simulations and experimental works to achieve a deeper understanding of the phase behavior [4–6]. In a parallel study, Kobayashi et al. [7] studied the Al and W diffusion in Co using Co-Al and Co-W alloys and annealing at different temperatures, demonstrating that γ' is metastable and γ , CoAl and Co_3W are in equilibrium at 900 °C. In fact, the amount, shape, and level of coarsening of the γ' precipitates are directly correlated with the creep properties of these alloys [8,9].

Numerous investigations were conducted to improve this family of Co-based superalloys' performance using various techniques. One was to adjust the amount of Al and W by increasing the γ' area stability, which in turn increased the γ' volume percentage [10–12]. Another one was to add Ni to Co-based superalloys due to the good dissolution of Ni in the Co lattice [13–16]. According to Shinagawa et al.'s studies [17], Ni stabilizes the γ phase. The amount of Ni can alter element partitioning and, in turn, the shape of the γ' , which is an important factor because any variation of shape is linked to a misfit change between γ and γ' [7,18]. Ti and Ta are the most effective alloying elements to induce an increase in the quantity of γ' if the goal is to increase its volume fraction. Furthermore, the rise in the volume of γ' and in the dissolving temperature of the γ' precipitates are also somewhat positively impacted by Nb and Hf addition.

The most common method of substantially modifying the features is by means of a small quantity of alloying elements [7,19–22]. For example, a number of recent studies describe substituting W or Al to improve the stability of the γ' area and even lower the alloy's density. Mo, Nb, or V have taken the role of W [23–26], and Ti and Ta have replaced Al [27,28]. The basal Co-9-9 alloy's high-temperature oxidation behavior can also be enhanced by small additions of Si and Cr [29].

Nearly all of the γ/γ' Co-based superalloys were produced through ingot casting. However, several studies have also employed the powder metallurgy (PM) approach because of its advantages over the melting process; this includes greater control over the microstructural characteristics to prevent unwanted secondary phase precipitation and segregation, uniform distribution of fine precipitates, and flexibility in selecting and developing alloy compositions. Further, the PM route enables the production of materials with small grain size, even in the nanometric range, with a high density of dislocations and high microstrain. This is achieved by mechanically milling the powders prior to consolidation. This high level of deformation after mechanical milling preserves the grain size after consolidation, although it requires sintering techniques that apply temperature and pressure simultaneously. In fact, the small grain size has an improvement in the final mechanical properties of the consolidated sample [30,31]. One possibility that offers the PM route is the development of harmonic structures. Ameyama et al. studied the density enhancement in different alloys (Co-Cr-Mo, Ti-based, etc.) with harmonic structure by the PM route [32–34]. A harmonic structure is composed of a core of larger grain sizes surrounded by a connected shell of smaller grain sizes. This kind of bimodal structure, in which the core grains cause an increase in strain and the shell grains cause an increase in stress, has also associated an improvement in the mechanical properties with the best balance between strength and toughness [35,36].

The main purpose of this work is to investigate the possibilities of improving the Co-9Al-9W (at.%) performance by developing harmonic structures and bimodal structures rather than by changing the chemical composition while working on the γ' stabilization.

2. Materials and Methods

The National University of Kongju (Chungcheongnam-do, Gongju, Korea) produced the prealloyed powders by gas atomizing (N_2) with the Co-9Al-9W (at.%) composition. Subsequently, the prealloyed powders underwent a low energy mechanical milling process to provide the harmonic structure. The low energy milling (LEM) process was performed for 10 h at 150 rpm under Ar atmosphere, using 10 mm stainless steel balls and 80 mL stainless steel vials with a ball to powder ratio of 1.8:1 (Table 1). Materials consolidated from the atomized powders were tagged as Co-9-9-At, and those obtained after the harmonic treatment as Co-9-9-At-Harmonic.

Table 1. Nomenclature and main milling parameters.

Atomizing Co-9-9-At	Low Energy Milling Co-9-9-At-Harmonic	
Gas atomizing N ₂	Milling tools	Stainless Steel
	Speed (rpm)	150
	Ball: Powder ratio (wt.)	1.8:1
	Atmosphere	Ar

To preserve the powder grain sizes as much as possible, milled powder was consolidated by a fast-sintering technique, in this case by spark plasma sintering (SPS), which is a field assisted sintering technique, using an HPD-25 equipment (FCT System GmbH, Germany) at Nanomaterials and Nanotechnology Research Center (“Centro de Investigación en Nanomateriales y Nanotecnología”—CINN, Asturias, Spain). Discs of approximately 20 mm diameter and 5 mm thickness were produced, with a heating rate of 100 °C/min and a dwell of 5 min at 1200 °C, under 80 MPa of pressure. The temperature was controlled by a pyrometer. W foil was used to cover the interior die surfaces in order to stop C diffusion from the graphite die during the consolidation process.

In order to promote the L12 phase precipitation, heat treatments were performed after sintering in a Carbolite HVT 15/50/450 furnace (Hope Valley, Derbyshire, UK) under high vacuum (10^{−5} mbar). First, a homogenization treatment was performed at 1250 °C for 24 h, followed by an ageing annealing treatment at 900 °C for 24 h. Heating and cooling rates were fixed at 5 °C/min.

X-ray diffraction (XRD) was used to investigate the lattice parameter, microstrain level, and crystallite size of both the powders and the consolidated materials in order to identify the primary phases that were formed (Empyrean, PANalytical, Kassel, Germany). To improve the accuracy in the determination of such parameters, the conditions of the measurements performed were 45 kV and 40 mA, with a step size of 0.0131°, and a measuring time per step of 438.345 s/step.

On every step of the processing route, microstructural analyses were performed using both a Zeiss Crossbeam 1540 focused ion beam (FIB) instrument with an Oxford Instruments EDX system and a FEG S/TEM (Talos F200X, FEI) transmission electron microscope (TEM). The SEM sample preparation involved gentle grinding with 1200- and 2000-grit sandpapers, followed by polishing with 9 and 3 μm diamond pastes and a 0.5 μm colloidal silica solution. The TEM sample preparation starts with a lamella (foil) extraction using a FIB, because the ion beam that is hitting the sample can mill and polish the surface giving a thin foil.

The γ' grain size was determined by image analysis using the software ImageJ from TEM images. The area of at least 50 grains was measured and its average size determined, considering Feret's diameter.

Thermogravimetric analyses (TGA) were carried out on a Q50 (TA Instruments, New Castle, DE, USA) with high-precision balance and a platinum sample pan. The equipment was used to calculate the Curie temperature of the powders and it was carefully calibrated with the Ni standard. A magnet was placed outside and under the TGA furnace to measure an apparent loss of weight produced from the change in attraction between the Ni sample and the magnet when temperature is increased above its Curie point. The onset of the curve is adjusted to agree with the material's known Curie point temperature, 358 °C (approximately).

The fraction of the alloying elements in the different phases of the microstructure were analyzed through EDX-TEM analysis (see Supplementary Materials) and by atom probe tomography (APT). APT specimens were fabricated with an FEI Nova 200 dual beam scanning electron microscope (SEM)/focused ion beam (FIB) instrument using the method described in [37]. The APT experiments were run using a CAMECA LEAP 4000XHR in voltage mode with a 50 K base temperature, 20% pulse fraction, 0.5% detection rate, and

a 200 kHz pulse repetition rate. The APT results were reconstructed and analyzed using CAMECA's IVAS 3.8 software.

Hardness and compression tests were carried out to define the mechanical properties of the sintered compacts. Compression tests were conducted from RT to high temperatures (600, 700, and 750 °C) using an Instron 3384 (Norwood, MA, USA) machine at a strain rate of $4 \times 10^{-3} \text{ s}^{-1}$ on a quadrangular sample ($2 \times 2 \times 4 \text{ mm}$ of dimensions). The hardness tests were carried out in a Vickers tests equipment (ZHV μ -Zwick Roell-) with 0.1 kgf force for 10 s and with a quadrilateral diamond pyramid indenter.

3. Results

3.1. Powder Characterization

Figure 1 displays SEM images of the powders after atomizing and LEM to produce the harmonic powders. It shows the spherical morphology (upper images) and the cross section of the gas-atomized powders (lower images). In Figure 1b it can be observed that a fully prealloyed grade is attained displaying a dendritic γ -fcc phase. Concerning the powder obtained after LEM, Co9-9-At-harmonic, Figure 1c shows that bigger particles maintain a spherical shape with some superficial deformation, and smaller powder particles display a flat shape. Cross sectional images show the differences between both states. The grain size of the powder after LEM is smaller in the edge than in the center of the powder particle (Figure 1d). The particles size of both powders varies from 10 to 100 μm in width.

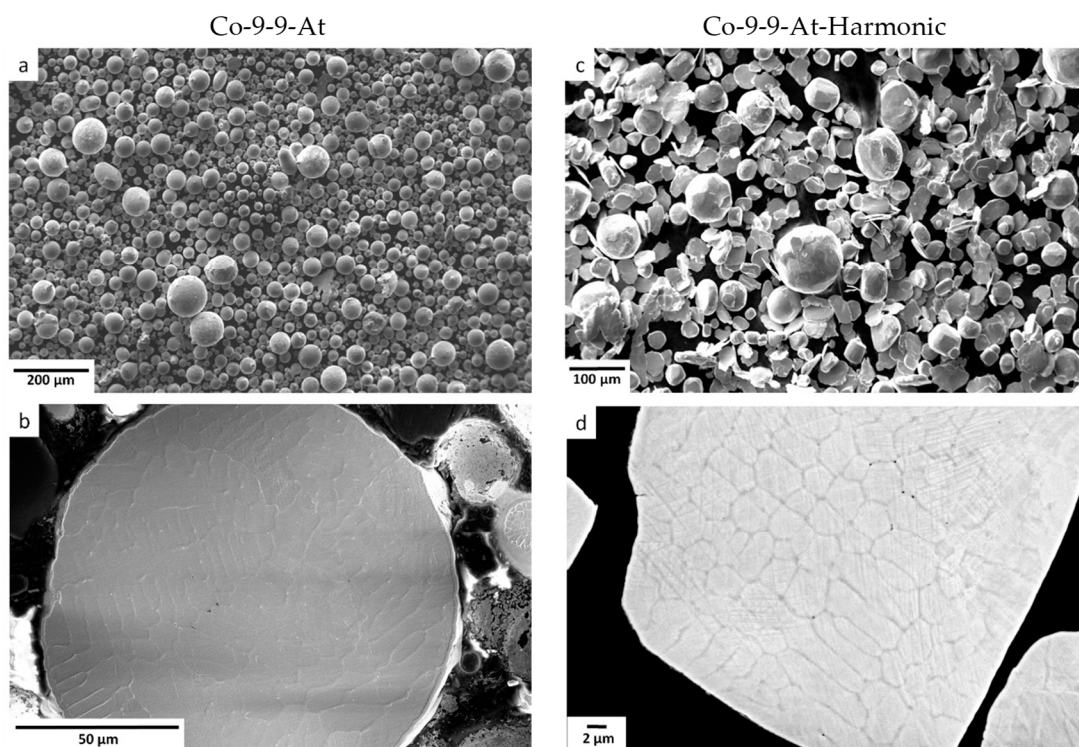


Figure 1. SEM images of Co-9Al-9W atomized powder (a,b) and Co-9Al-9W harmonic powder (c,d).

The XRD patterns of the atomized powders show the phases present in the powder and enable the determination of structural parameters such as crystallite size (L), microstrain ($\langle \varepsilon^2 \rangle^{1/2}$) and cell parameter (a) (see Figure 2 and Table 2). Pure Co powders were added to Table 2 for comparison. Atomized and harmonic powders display a single phase, γ -fcc. However, in the harmonic powders two small peaks at 41° and 43° can be depicted, which could belong to some hcp clusters that were formed after the low energy milling process.

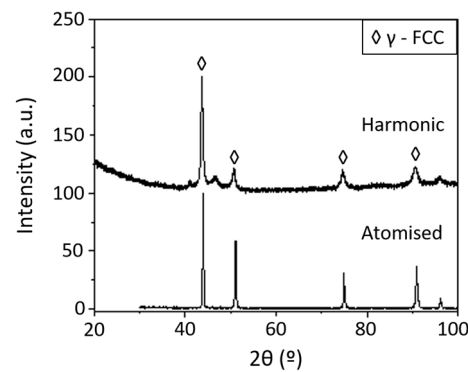


Figure 2. Diffractogram of atomized (lower) and harmonic powders (upper).

Table 2. Structural features of pure fcc-Co powder, atomized Co-9-9 powder, and atomized Co-9-9 powder after LEM.

Sample	Plane (1 1 1) of γ -Phase		
	L (nm)	$\langle \varepsilon^2 \rangle^{1/2} \cdot 10^{-3}$	a (Å)
Pure fcc-Co	12.2	0.005	3.540
Co-9-9-At	26.6	0.002	3.567
Co-9-9-At-Harmonic	12.6	0.005	3.588

A method for examining the powder modification using LEM involves determining the structural characteristics (crystallite size and microstrain level) while taking into account the (111) plane of the γ -fcc phase, which is the most intense peak on the diffractogram (Figure 2). The outcomes are compared to the pure Co-fcc powder (Table 2).

As it is expected in the harmonic powder, the crystallite size decreases and the microstrain increases compared to the atomized powder. The deformed particles show an increase in the concentration of lattice defects that distort the order and lattice of the unit cell. The level of distortion promotes the increase in the microstrain value, and the decrease in the crystallite size. The increase in the unit cell parameter is also linked to the distorted cell as well as the increment of the lattice parameter. In comparison to the milled Co-9-9-Harmonic and pure Co powder, the fully prealloyed grade produced by atomization has a larger crystallite size, a more homogenous composition, and a lower strain level.

The Curie temperature is influenced by the composition and structural properties as well, so the alloy grade and powder deformation can be confirmed by measuring this parameter by TGA (Table 3).

Table 3. Curie temperature of pure fcc-Co, Co-9-9-At and Co-9-9-At-Harmonic powders determined by TGA.

Material	Curie T (°C)
Pure powder Co-fcc	470
Co-9-9-At	260
Co-9-9-At-Harmonic	350

To comprehend the evolution of this parameter, two phenomena need to be considered. When Al and W are involved, the Curie temperature will drop as the solute content rises. On the other hand, the lattice defects created by the milling process harden the diamagnetic moment's alignment and raise the Curie temperature. When the elemental Co-powder is compared to the Co-9-9-At and Co-9-9-At-Harmonic powders, both effects are evident. The alloying elements effect, which lowers the Curie temperature, is reported in the Co-9-9-At instance. In the case of Co-9-9-At-Harmonic powder, the lattice distortion is evident when

the Curie temperature rises in comparison to Co-9-9-At powder; nonetheless, it remains lower than the Curie temperature of pure Co-fcc powder.

3.2. Microstructural Evolution of Consolidated Specimens

Both powders, Co9-9-At and Co-9-9-At-Harmonic, were consolidated by SPS and heat treated (homogenized and aged) to attain a dual γ/γ' microstructure. Figure 3 displays the evolution of the consolidated samples (a, b, g, h), after both thermal treatments, homogenization (c, d, i, j) and aging (e, f, k, l). The evolution of both samples is similar in terms of γ' volume fraction. Table 4 collects the size and volume fraction of the γ' precipitates for each consolidation stage.

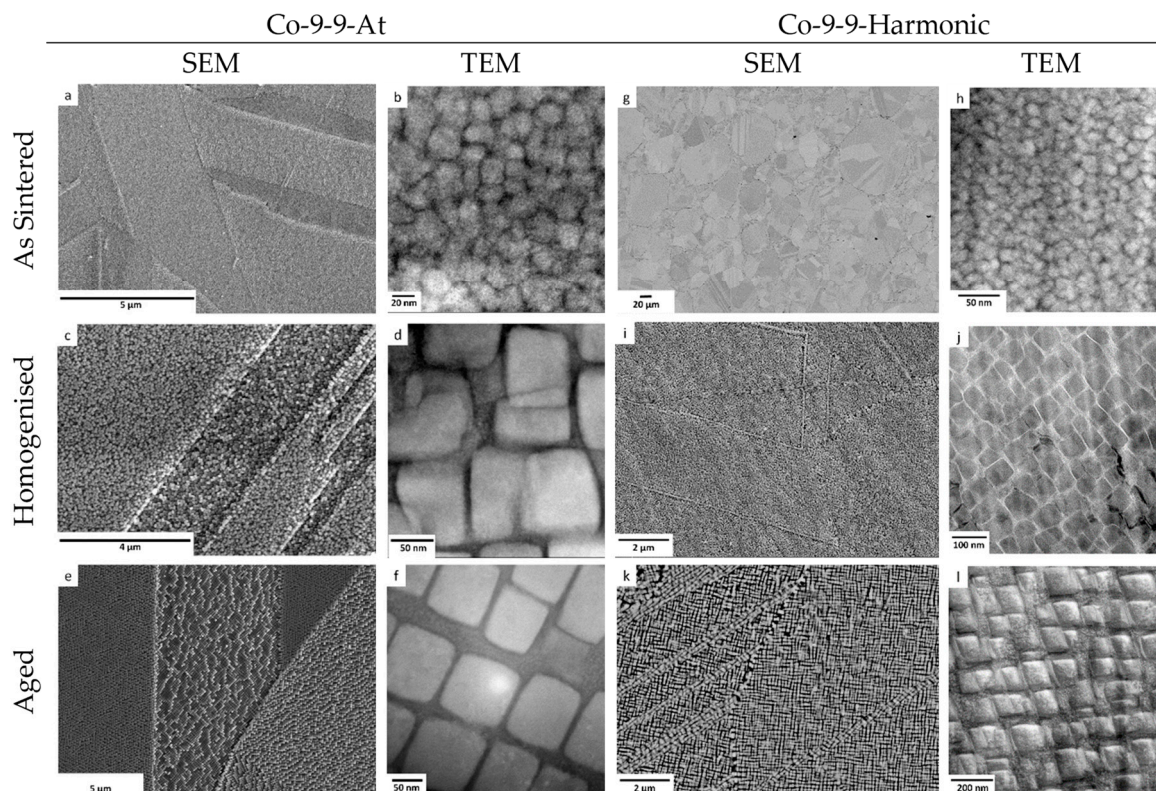


Figure 3. SEM and TEM images of Co9-9-At and Co-9-9-Harmonic-sintered alloys in the three stages, as-sintered, homogenized (1250 °C for 24 h), and aged (900 °C for 24 h). (a) As sintered SEM Image Co-9-9-At; (b) As sintered TEM image Co-9-9-At; (c) Homogenized SEM Image CO-9-9-At; (d) Homogeized TEM Image Co-9-9-At; (e) Aged SEM Image Co-9-9-At; (f) Aged TEM Image Co-9-9-At; (g) As sintered SEM Image Co-9-9-Harmonic; (h) As sintered TEM image Co-9-9-Harmonic; (i) Homogenized SEM Image CO-9-9-Harmonic; (j) Homogeized TEM Image Co-9-9-Harmonic; (k) Aged SEM Image Co-9-9-Harmonic; (l) Aged TEM Image Co-9-9-Harmonic.

Table 4. γ' size and volume fraction for the different processing conditions.

Sample	γ' Size (nm)		
	As-Sintered	Homogenized	Aged
Co-9-9-At	28 ± 5	106 ± 15	146 ± 26
Co-9-9-At-Harmonic	19 ± 4	75 ± 13	173 ± 30
Sample	γ' volume fraction		
	As-sintered	Homogenized	Aged
Co-9-9-At	75%	71%	65%
Co-9-9-At-Harmonic	82%	76%	59%

After the first stage, as-sintered γ' precipitates were already present without any subsequent heat treatment. These precipitates display a small size (24 nm approx. in average) but a high-volume fraction (75%). It is noticeable how the γ' precipitates display different density and orientation in the regions divided by twin planes.

Following the homogenization treatment, the γ' precipitates in the Co-9-9 At samples grew four times, on average, from 28 to 106 nm in size, taking on a cuboidal form. Eventually, ageing heat treatment caused the γ' precipitates to orient in accordance with the original γ grain, resulting in a larger more cuboidal γ' precipitate (about 150 nm in size, see Figure 4), along with a decrease in volume fraction of these primary γ' cuboids.

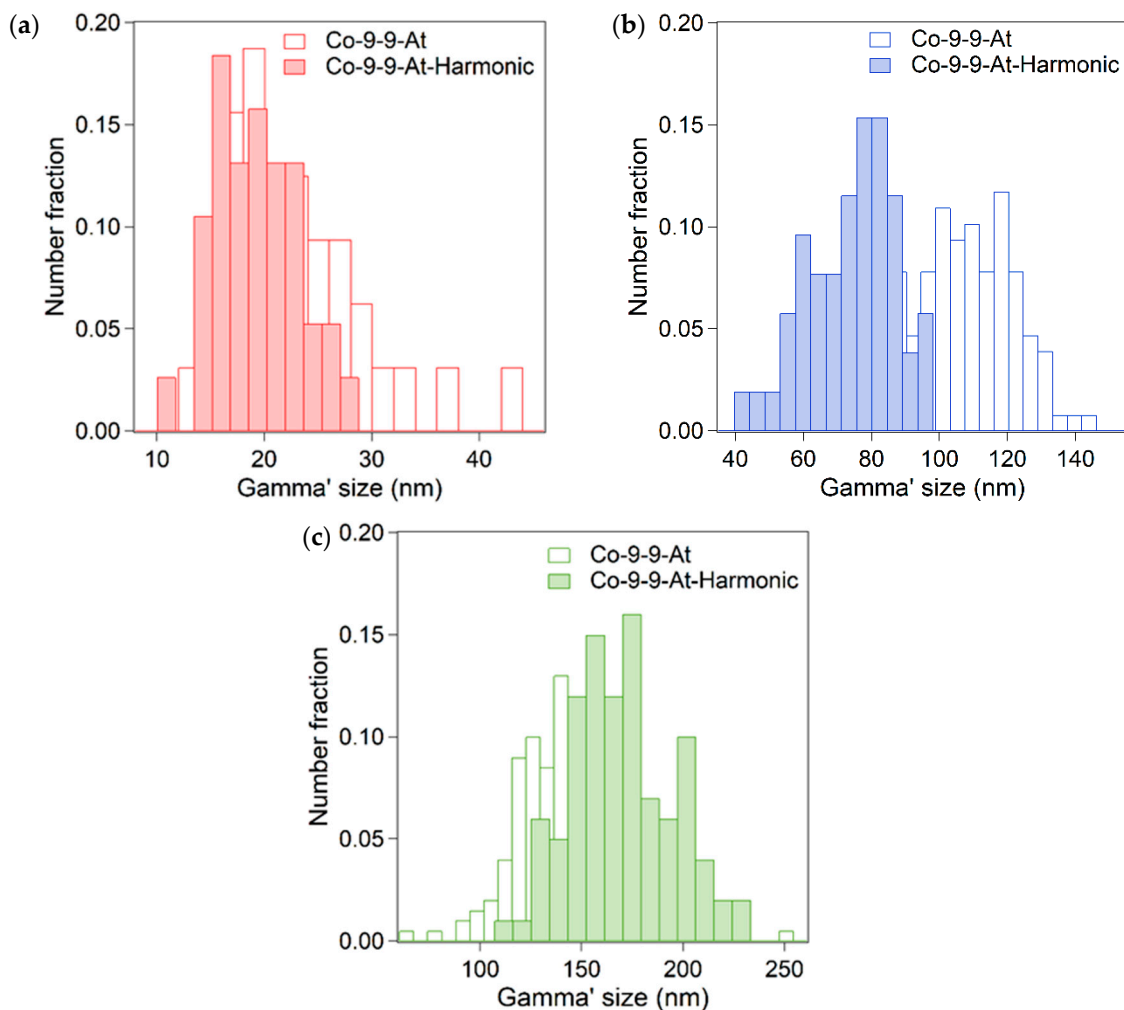


Figure 4. Grain size distribution of γ' particles in the (a) as-sintered state, (b) after homogenization at 1250 °C for 24 h, and (c) after ageing at 900 °C for 24 h.

Similar to the other samples, the γ' precipitates in the Co-9-9-At-Harmonic material have grown due to the ageing treatment. However, because of the high energy that was retained in the lattice during the LEM process, the growth multiplied eight times its initial size (refer to Table 4).

Overall, the alloys produced from atomized powder are free of secondary precipitates after consolidation and heat treatments. A comparison of the two samples concerning γ' size can be observed in Figure 4. Two different aspects can be highlighted: there is an increase in the average size of the γ' precipitates with the heat treatments, and a clear decrease in the average size when LEM is performed prior to consolidation. In the aged samples, however, the size of the γ' precipitates are more similar.

The elemental partitioning of the Co, Al and W in the present phases has also been studied using APT (Figure 5). Results have shown that Co is preferentially allocated in the γ phase, while the W and Al are preferentially allocated in γ' . The three-dimensional elemental maps together with the concentration profile along the interface of γ/γ' confirm the elemental distribution. Thanks to the APT, the interdiffusion area in the γ/γ' interface can be detected with a higher Al concentration.

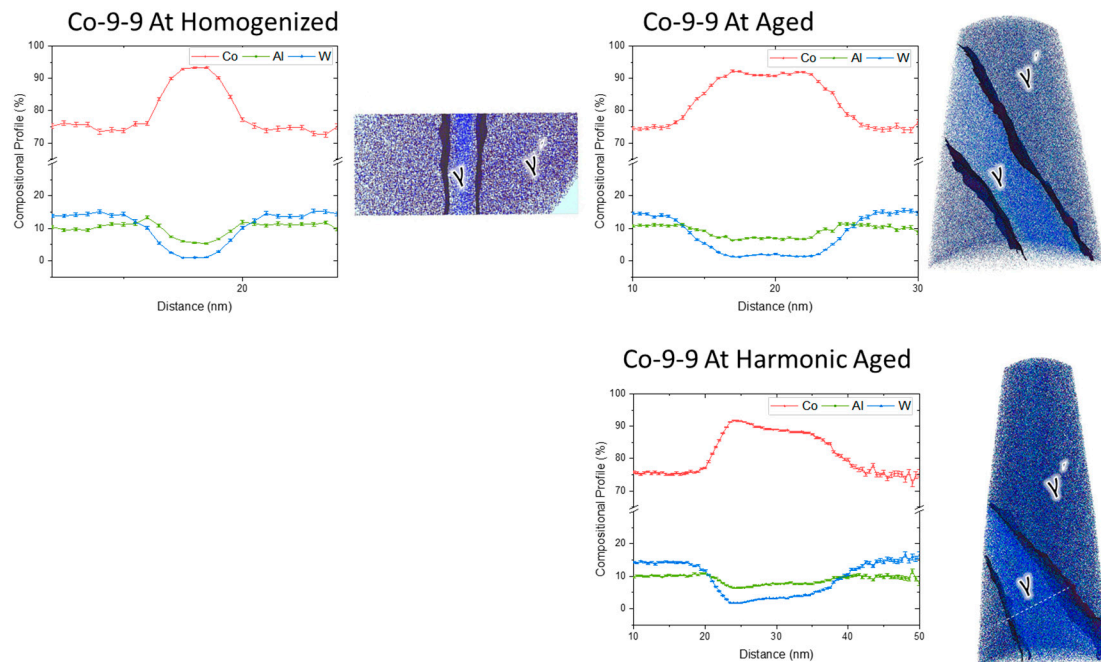


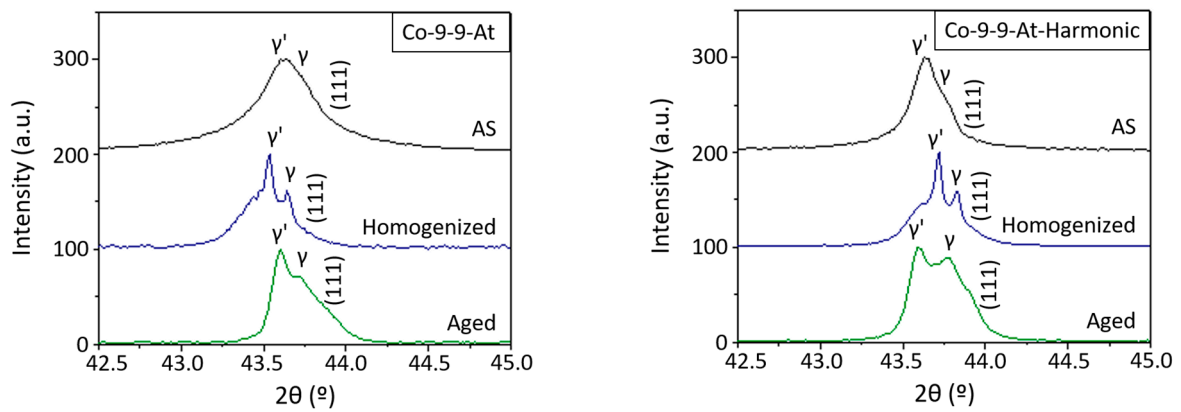
Figure 5. APT results for Co-9-9-At (homogenized and aged) and Co-9-9-At-Harmonic after aging. The APT atom maps have 10 at.% W iso-concentration surfaces.

This element distribution among the γ/γ' dual phase, may give an idea of the hardening due to the alloying effect. The enrichment in W of γ' could improve the mechanical properties of these alloys favoring the γ' hardening mechanism. This elemental distribution is similar in the as sintered and homogenized samples, where the γ' size and distribution make the elemental analysis vague.

The evolution of the γ' precipitates in the three stages defined above (as-sintered, homogenized, and aged) is studied by XRD regarding the misfit parameter, δ (Equation (1)). This parameter defines the coherency between γ and γ' , which according to Mughrabi [38], helps to predict the mechanical behavior of the alloy at high temperatures, being more favorable with positive δ due to the activation of the twins' movements through the parallel channels to the strain.

$$\delta = \frac{2(a_{\gamma'} - a_{\gamma})}{a_{\gamma'} + a_{\gamma}} \quad (1)$$

The δ study has been made using the most intense peak of the fcc crystal structure that belongs to the (111) plane (Figure 6). It can be observed how the position of the (111) XRD peak corresponding to γ and γ' evolves as the Co alloy is treated with different thermal cycles. The heat treatments effect on the superalloys processed from atomized powders depends on the attained homogenization degree, and therefore the peaks move to lower angles. Once the material is aged, the shape and the size of γ' can change, decreasing the distortion of the lattice, and hence the relaxation is translated in the XRD peaks into higher value angles. Hence, the δ values show how the heat treatments affect the size and shape of the γ' precipitates; a larger δ results in less coherency between γ and γ' and a more cuboidal γ' .



Misfit (δ)	As-Sintered	Homogenized	Aged
Co-9-9-At	0.07	0.24	0.24
Co-9-9-At-Harmonic	0.05	0.24	0.38

Figure 6. Detailed XRD of the most intense peak of the γ and γ' phases—(111) plane—for both consolidated materials. Misfit values regarding alloy and processing steps.

3.3. Mechanical Properties

Figure 7 shows the microhardness values of the materials after consolidation and heat treatment. It can be observed that the values of samples consolidated from harmonic powders are higher than samples processed from the atomized powders.

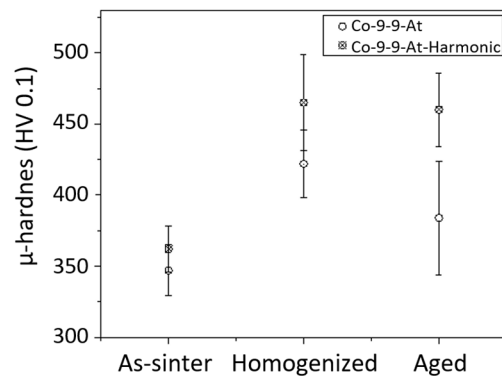


Figure 7. Microhardness of the processed materials.

The microhardness level is improved by heat treatments, but the maximum value is attained after homogenization and does not increase further with aging. This is confirmed by the microstructural evolution shown in Figure 3.

In Figure 8, we can compare the compression yield stress for the different materials and tests at different temperatures. The graph also displays comparison results for a traditional Ni-based superalloy and the Co superalloy made by ingot casting, as referenced in [2,39]. Compared to the reference materials, all the materials in this study exhibit significant improvements in terms of high yield stress values. In accordance with the hardness measurement trend, Co-9-9-At-Harmonic-Aged and Co-9-9-At-Homogenized materials exhibit the greatest values.

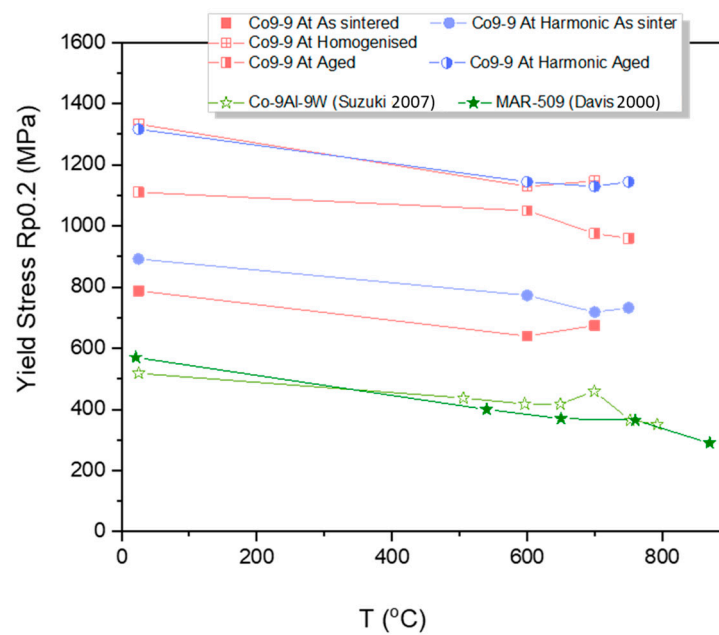


Figure 8. Compression yield stress as a function of test temperature for all the studied materials and some reference materials.

4. Discussion

4.1. Structural and Microstructural Features

The structural features of consolidated and heat-treated samples have been investigated in depth by XRD (Figures 2 and 6). The results show that after heat treatments (homogenization and ageing), despite the overlap of the peaks, the maximum of each peak is clearly defined, and enables the individual study of each phase. The shift of the peaks to lower values of 2θ after homogenization treatment in sample Co-9-9-At-Homogenized, indicates an increase in the lattice parameters explained by the activation of atomic movement during homogenization. However, this shift is not observed for sample Co-9-9-At-Harmonic-Homogenized, possibly due to the residual strain present in the as-sintered samples, as a consequence of the LEM process. Concerning the effect of the aging treatment, it produces a split of the peaks towards lower 2θ angles that indicate a decrease in the lattice parameters. During the ageing heat treatment, the temperature may not be enough to favor atomic movement, but the γ' could grow instead of the γ phase.

The proportion of each phase is revealed by the peaks' relative intensities. The superposition of peaks in the as-sintered samples conceals the effect of homogenization. The fraction of γ' decreases with aging, as seen by the lower difference between the highest values of the two peaks, although there is still a noticeable effect. These findings concur with the TEM observations that were gathered and are listed in Table 4.

Microstructural analysis (Figure 3) can be used to confront the impact of the heat treatments on the size and shape of the γ' precipitates in light of the misfit results (δ) (Figure 6). The sample exhibits a large precipitation of a very small (~ 20 nm) rounded γ' phase in the as-sintered stage, with a very low related misfit value indicating a high degree of coherence with the γ -matrix.

The homogenized sample can be examined using SEM and TEM to observe the progression of the γ' precipitates and their evolution toward a more cuboidal shape, which is linked to an increase in the δ value. Now, the cuboids are 50–100 nm in size. Detailed observations reveal that secondary γ' can be found mixed in with the initial γ' precipitates at the prior γ channels. Following the precipitation mechanism outlined in [40–42], precipitation of these secondary γ' (with a size below 10 nm) could happen during cooling. Even though the energy needed for growth is greater than the energy needed for nucleation, both

processes happened during the heat treatment. However, nucleation rather than growth is encouraged during the cooling step, promoting the secondary γ' formation.

In the aged sample, the γ' is oriented according to the previous γ grain orientation. As an example, in Figure 3e there are three different γ' orientations, which agree with different prior γ grains.

At the grain boundaries there are some chaotic precipitation events due to the precipitate reorientation. The TEM image (Figure 3f) displays a pristine γ' orientation, with nicely organized γ' precipitates that have a cuboidal shape and a size of about 100 nm. The orientation of the γ' is affected by aging, and its size is comparable to that of the homogenized sample. Furthermore, the distance between primary γ' is greater than that of the homogenized sample that contained secondary γ' precipitates in the distances between γ' , which were smaller than 10 nm.

With the aim to verify the cubic structure of γ and γ' , the area presented in Figure 9 was oriented in the $[\bar{1}\bar{1}\bar{2}]$ zone axis. The diffraction pattern of this area is presented in the upper right corner of Figure 5, where there are two lattices with different intensity in the reflections. These two shifted lattices contain a typical diffraction pattern from a γ/γ' dual phase because the γ' precipitates have coherent interfaces with the γ matrix. To disclose the belonging of each lattice, the reflection marked with a red circle was chosen to take an image in the bright field mode (Figure 5, bottom right). The brighter areas are the ones that produce the chosen reflection, so the reflections with less intensity belong to γ' precipitates because they have white contrast in the image.

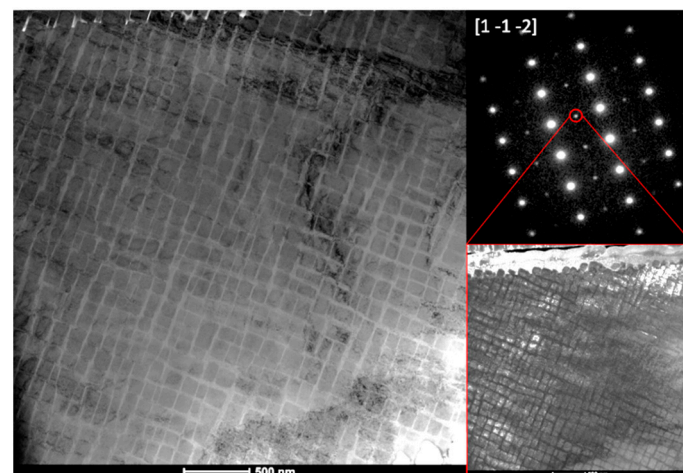


Figure 9. Bright field TEM image of the γ/γ' area in the Co-9-9-At aged sample, diffraction pattern in the $[\bar{1}\bar{1}\bar{2}]$ zone axis (upper right image), and image of selected diffracted beam (lower right image).

The similarity of the lattice parameters of γ and γ' make it difficult to be calculated by TEM.

4.2. Effect of Harmonic Structure in Atomized Alloys

As it was previously stated, the LEM activates the powder surface and creates a harmonic structure with a core-shell structure. After the consolidation process, the structure is composed of γ -fcc and γ' -L12 phases (Figure 3), free of secondary precipitates. The phases' evolution follows the same pattern as the alloys outlined for the atomized Co-9-9 materials; however, in certain cases, such as the homogenized samples, the relative intensity of the γ' peaks is higher since there are more and larger precipitates.

Figure 2 shows the most intense peak, corresponding to the (111) plane for both phases. Figure 6 illustrates how the milling process creates a highly distorted lattice, which facilitates γ' precipitation and allows for greater γ' precipitation as a result of the heat treatments. The maximum of the peaks is clearly determined after the heat treatments, however because of the lattice similarities and phase coherency, the peaks always overlap.

The coherency of those phases is analyzed by means of misfit value. A shift towards semi-coherent precipitates, which will aid in the material's hardening, is indicated by increasing δ values from the as-sintered stage to homogenization and ageing treatments.

Figure 3 illustrates how the harmonic microstructure has evolved, showing how the γ' precipitate has grown larger and more cuboidal. Moreover, a huge precipitation of secondary γ' (which is not represented in the value of the volume fraction of γ' in Table 4) can also be identified and will contribute to the different behavior under load since it is in charge of the dislocations' decreased mobility.

The as sintered samples show round ~ 20 nm sized γ' randomly precipitated throughout the bulk, which is similar to the alloys produced from atomized powder directly. But homogenized samples have a larger γ' size (~ 50 – 100 nm) with a bigger distance between primary γ' cuboids, where secondary γ' precipitates with less than 10 nm sizes appear. This increase in the primary γ' distance is due to atomic movement during ageing that promotes an elemental concentration gradient [40–42].

4.3. Mechanical Properties

The two processed PM alloys offer a unique opportunity to explore the principal hardening mechanism of γ' precipitation by achieving a plain dual γ - γ' microstructure, free of secondary phases.

There is a parallel evolution of microhardness values and γ' sizes. In the case of Co-9-9-At, the highest value corresponds to the homogenized sample due to the growth of cuboids from 20 to 100 nm. In the case of aged samples, the hardness values are maintained with less uncertainty. Due to the deformation induced by the low energy milling process, the Co-9-9-At-harmonic samples display higher hardness (Figure 8).

Because the smallest γ' size can prevent dislocation movement, the dual γ' size (20 and 170 nm approximately) that precipitated in the Co-9-9-At-Harmonic samples could retain the material's hardness.

The mechanical response of the material has been greatly impacted by the low-energy milling process, (Co-9-9-At-Harmonic) which has also increased the density of structural defects in the material in addition to inducing plastic deformation of the particle surface. The diffusion processes between the particles that control grain size have been triggered by the plastic deformation, and the lattice defects have created the possibility of additional potential nucleation sites for further γ' precipitates. Moreover, this has favored greater γ' secondary precipitation in these materials.

The values of the yield stress (Y.S.) help to understand the mechanical behavior of the materials with respect to the temperature and allow an easier comparison between the Co-based alloys produced by different methods (Figure 9). Here, the Co-9-9-At alloys behave better than reported Co-based alloys such as MAR-509 [39] and Co-9Al-9W [2], even more so when the samples are heat treated.

MAR-509 is a commercial Co-based superalloy produced by ingot casting with the composition: Cr: 22.5–24.35, Ni: 9–11, W: 6.5–7.5, C (max): 0.55–0.65, others (Ti, Ta, B, B, Zr, etc.) [39]. In this case, solid solution hardening and carbide formation are the main strengthening mechanisms. The other reference, the alloy Co-9Al-9W that Suzuki et al. [2] suggested, has the same composition but was produced by induction melting. It was then heat treated for 12 h at 1350 °C and aged for 150 h at 900 °C to precipitate γ' .

The evolution of the Y.S. with temperature of the as-sintered Co-9-9-At alloy is clearly superior to the behavior of the MAR-509 [39] and the Co-9Al-9W alloys [2]. This is a very remarkable result since the shape, size, and coherence of the precipitates are not yet optimal at this stage. By means of heat treatment of the samples, the values currently reported for these alloys can be doubled.

At around 700 °C for Co-9-9-At alloys and 750 °C for harmonic alloys, the “so-called” anomalous Y.S. behavior has been detected. The achievement of this anomalous behavior, without additional alloying elements, at higher temperatures than those reported is an

improvement due to the fact that the range of materials that can be used is superior to that of other Co-based superalloys described [2,11].

These alloys are excellent choices for high temperature applications because of their final microstructure, which is free of secondary phases, and their incredibly ultra-fine grain size, which allows for the preservation of mechanical properties with temperature.

5. Conclusions

- When using atomized powder, γ' is formed during the SPS consolidation process without the need for subsequent heat treatment.
- This method prevents the precipitation of secondary phases, resulting in a fully dual γ/γ' microstructure.
- The orientation of γ' is altered by the ageing heat treatment based on the prior γ grain orientation.
- The energy required to precipitate γ' phases is easily increased after low energy milling due to the activation of the distorted matrix. The promotion of γ' precipitation is facilitated by the harmonic structure.
- The increase in δ misfit value in the aged harmonic samples suggests an effective hardening mechanism.
- Low energy milling also promotes a γ/γ' microstructure without secondary phases.
- The mechanical properties of the free secondary alloys produced from atomized powders remain high at high temperatures, exhibiting the so-called anomalous behavior at around 700 °C.
- The mechanical properties are significantly increased by the deformation lattice produced by LEM, even exhibiting anomalous behavior at higher temperatures, around 750 °C.
- The material hardness is slightly decreased by the γ' orientation that occurs after the ageing heat treatment.
- The mechanical behavior is not affected by the nominal composition of the studied alloys, at least when it is a ternary alloy with a low number of alloying elements.

Supplementary Materials: The following supporting information can be downloaded at: <https://www.mdpi.com/article/10.3390/met14010070/s1>. The original contributions presented in the study are included in the article and supplementary material, further inquiries can be directed to the corresponding author.

Author Contributions: Conceptualization, M.C. and J.M.T.; methodology, M.C., L.G.d.I.C. and J.M.T.; validation, M.C., M.C.-C., L.G.d.I.C., F.G.C., J.D.P. and J.M.T.; analysis, M.C., M.C.-C., L.G.d.I.C., F.G.C., J.D.P. and J.M.T.; investigation, M.C.-C., L.G.d.I.C. and J.D.P.; resources, M.C. and J.M.T.; writing—original draft preparation, M.C., M.C.-C. and J.M.T.; writing—review and editing, M.C., M.C.-C., L.G.d.I.C., F.G.C., J.D.P. and J.M.T.; funding acquisition, M.C. and J.M.T. All authors have read and agreed to the published version of the manuscript.

Funding: The author L. García de la Cruz received funding from the “Call for Grants for the requalification of the Spanish university system for 2021-2023”, from the Carlos III University of Madrid, of July 1, 2021. The research was supported by funding from the Madrid region under the program S2018/NMT-4381 with the MAT 4.0-CM Project, Spain. ATP research was supported by Center for Nanophase Materials Science. U.S. Department of Energy (DOE) Scientific User Facilities Division—Ref. CNMS2019-201.

Data Availability Statement: The data that support the findings of this study are available from the corresponding author, [J.M.T.], upon reasonable request.

Acknowledgments: Gas atomized powders were manufactured at Nacional University of Kongju (Korea). SPS was performed at the Nanomaterials and Nanotechnology Research Center (“Centro de Investigación en Nanomateriales y Nanotecnología”)—CINN, Asturias, Spain. APT research was supported by the Center for Nanophase Materials Sciences (CNMS), which is a US Department of Energy, Office of Science User Facility at Oak Ridge National Laboratory. The authors would like to thank James Burns for assistance in performing APT sample preparation and running the

APT experiments. This manuscript has been authored by UT-Battelle, LLC under Contract No. DE-AC05-00OR22725 with the U.S. Department of Energy. The United States Government and the publisher retain that by accepting the article for publication, the United States Government retains a non-exclusive, paid-up, irrevocable, world-wide license to publish or reproduce the published form of this manuscript, or allow others to do so, for United States Government purposes. The Department of Energy will provide public access to the results of federally sponsored research in accordance with the DOE Public Access Plan (<https://www.energy.gov/doe-public-access-plan> (accessed on 5 January 2024).

Conflicts of Interest: The authors declare no conflicts of interest.

References

1. Sato, J.; Omori, T.; Oikawa, K.; Ohnuma, I.; Kainuma, R.; Ishida, K. Cobalt-Base High-Temperature Alloys. *Science* **2006**, *312*, 90–91. [[CrossRef](#)] [[PubMed](#)]
2. Suzuki, A.; DeNolf, G.C.; Pollock, T.M. Flow Stress Anomalies in γ/γ' Two-Phase Co–Al–W-Base Alloys. *Scr. Mater.* **2007**, *56*, 385–388. [[CrossRef](#)]
3. Cui, Y.F.; Zhang, X.; Xu, G.L.; Zhu, W.J.; Liu, H.S.; Jin, Z.P. Thermodynamic Assessment of Co–Al–W System and Solidification of Co-Enriched Ternary Alloys. *J. Mater. Sci.* **2011**, *46*, 2611–2621. [[CrossRef](#)]
4. Yao, Q.; Xing, H.; Sun, J. Structural Stability and Elastic Property of the L1₂ Ordered Co₃(Al,W) Precipitate. *Appl. Phys. Lett.* **2006**, *89*, 161906. [[CrossRef](#)]
5. Jiang, C. First-Principles Study of Co₃(Al,W) Alloys Using Special Quasi-Random Structures. *Scr. Mater.* **2008**, *59*, 1075–1078. [[CrossRef](#)]
6. Ishida, K. Intermetallic Compounds in Co-Base Alloys-Phase Stability and Application to Superalloys. *MRS Online Proc. Libr.* **2008**, *1128*, 606. [[CrossRef](#)]
7. Kobayashi, S.; Tsukamoto, Y.; Takasugi, T.; Chinen, H.; Omori, T.; Ishida, K.; Zaefferer, S. Determination of Phase Equilibria in the Co-Rich Co-Al-W Ternary System with a Diffusion-Couple Technique. *Intermetallics* **2009**, *17*, 1085–1089. [[CrossRef](#)]
8. Chen, J.; Guo, M.; Yang, M.; Liu, L.; Zhang, J. Double Minimum Creep Processing and Mechanism for γ' Strengthened Cobalt-Based Superalloy. *J. Mater. Sci. Technol.* **2022**, *112*, 123–129. [[CrossRef](#)]
9. Chen, J.; Guo, M.; Yang, M.; Su, H.; Liu, L.; Zhang, J. Phase-Field Simulation of Γ' Coarsening Behavior in Cobalt-Based Superalloy. *Comput. Mater. Sci.* **2021**, *191*, 110358. [[CrossRef](#)]
10. Miura, S.; Ohkubo, K.; Mohri, T. Mechanical Properties of Co-Based L1₂ Intermetallic Compound Co₃(Al,W). *Mater. Trans.* **2007**, *48*, 2403–2408. [[CrossRef](#)]
11. Shinagawa, K.; Omori, T.; Oikawa, K.; Kainuma, R.; Ishida, K. Ductility Enhancement by Boron Addition in Co-Al-W High-Temperature Alloys. *Scr. Mater.* **2009**, *61*, 612–615. [[CrossRef](#)]
12. Suzuki, A.; Pollock, T.M. High-Temperature Strength and Deformation of γ/γ' Two-Phase Co–Al–W-Base Alloys. *Acta Mater.* **2008**, *56*, 1288–1297. [[CrossRef](#)]
13. Singh, M.P.; Olu, E.F.; Pandey, P.; Chattopadhyay, K. Thermophysical and Magnetic Properties of Co-Ni-Mo-Al-Ta Class of Tungsten Free Co-Based Superalloys. *J. Alloys Compd.* **2021**, *879*, 160379. [[CrossRef](#)]
14. Long, F.R.; Baik, S.I.; Chung, D.W.; Xue, F.; Lass, E.A.; Seidman, D.N.; Dunand, D.C. Microstructure and Creep Performance of a Multicomponent Co-Based L1₂-Ordered Intermetallic Alloy. *Acta Mater.* **2020**, *196*, 396–408. [[CrossRef](#)]
15. Chung, D.-W.; Toinin, J.P.; Lass, E.A.; Seidman, D.N.; Dunand, D.C. Effects of Cr on the Properties of Multicomponent Cobalt-Based Superalloys with Ultra High γ' Volume Fraction. *J. Alloys Compd.* **2020**, *832*, 154790. [[CrossRef](#)]
16. Lass, E.A. The Effects of Fe and Si on the Phase Equilibria in a γ' -Strengthened Co–Al–W-Based Superalloy. *J. Alloys Compd.* **2020**, *825*, 154158. [[CrossRef](#)]
17. Shinagawa, K.; Omori, T.; Sato, J.; Oikawa, K.; Ohnuma, I.; Kainuma, R.; Ishida, K. Phase Equilibria and Microstructure on γ' Phase in Co-Ni-Al-W System. *Mater. Trans.* **2008**, *49*, 1474–1479. [[CrossRef](#)]
18. Omori, T.; Oikawa, K.; Sato, J.; Ohnuma, I.; Kattner, U.R.; Kainuma, R.; Ishida, K. Partition Behavior of Alloying Elements and Phase Transformation Temperatures in Co-Al-W-Base Quaternary Systems. *Intermetallics* **2013**, *32*, 274–283. [[CrossRef](#)]
19. Ooshima, M.; Tanaka, K.; Okamoto, N.L.; Kishida, K.; Inui, H. Effects of Quaternary Alloying Elements on the γ' Solvus Temperature of Co-Al-W Based Alloys with Fcc/L1₂ Two-Phase Microstructures. *J. Alloys Compd.* **2010**, *508*, 71–78. [[CrossRef](#)]
20. Mottura, A.; Janotti, A.; Pollock, T.M. A First-Principles Study of the Effect of Ta on the Superlattice Intrinsic Stacking Fault Energy of L1₂-Co₃(Al,W). *Intermetallics* **2012**, *28*, 138–143. [[CrossRef](#)]
21. Mottura, A.; Janotti, A.; Pollock, T.M. Alloying Effects in the Gamma Prime Phase of Co-Base Superalloys. In Proceedings of the Superalloys 2012: 12th International Symposium on Superalloys, Seven Springs, PA, USA, 9–13 September 2012; pp. 685–693. [[CrossRef](#)]
22. Xue, F.; Wang, M.; Feng, Q. Alloying Effects on Heat-Treated Microstructure in Co-Al-W-Base Superalloys at 1300 °C and 900 °C. *Superalloys* **2012**, *2012*, 813–821. [[CrossRef](#)]

23. Makineni, S.K.; Samanta, A.; Rojhirunsakool, T.; Alam, T.; Nithin, B.; Singh, A.K.; Banerjee, R.; Chattopadhyay, K. A New Class of High Strength High Temperature Cobalt Based γ - γ' Co-Mo-Al Alloys Stabilized with Ta Addition. *Acta Mater.* **2015**, *97*, 29–40. [[CrossRef](#)]
24. Davydov, D.; Kazantseva, N.; Ezhov, I.; Popova, E. Effect of Alloying on the γ - γ' Microstructure of W-Free Co-Based Superalloys. *Mater. Today Proc.* **2021**, *38*, 1971–1973. [[CrossRef](#)]
25. Reyes Tirado, F.L.; Taylor, S.V.; Dunand, D.C. Low-Density, W-Free Co-Nb-V-Al-Based Superalloys with γ/γ' Microstructure. *Mater. Sci. Eng. A* **2020**, *796*, 139977. [[CrossRef](#)]
26. Reyes Tirado, F.L.; Dunand, D.C. Increasing γ' Volume Fraction in Co-Nb-V- and Co-Ta-V-Based Superalloys. *J. Mater. Res. Technol.* **2021**, *11*, 2305–2313. [[CrossRef](#)]
27. Liu, X.; Chen, Z.; Chen, Y.; Yang, S.; Pan, Y.; Lu, Y.; Qu, S.; Li, Y.; Yang, Y.; Wang, C. Multicomponent Co-Ti-Based Superalloy with High Solvus Temperature and Low Lattice Misfit. *Mater. Lett.* **2021**, *284*, 128910. [[CrossRef](#)]
28. Im, H.J.; Choi, W.S.; Ryou, K.; Seol, J.B.; Kang, T.H.; Ko, W.-S.; Choi, P.-P. Enhanced Microstructural Stability of γ/γ' -Strengthened Co-Ti-Mo-Based Alloys through Al Additions. *Acta Mater.* **2021**, *214*, 117011. [[CrossRef](#)]
29. Liang, Z.; Göken, M.; Lorenz, U.; Neumeier, S.; Oehring, M.; Pyczak, F.; Stark, A.; Wang, L. Influence of Small Amounts of Si and Cr on the High Temperature Oxidation Behavior of Novel Cobalt Base Superalloys. *Corros. Sci.* **2021**, *184*, 109388. [[CrossRef](#)]
30. Cartón-Cordero, M.; Campos, M.; Freund, L.P.; Kolb, M.; Neumeier, S.; Göken, M.; Torralba, J.M. Microstructure and Compression Strength of Co-Based Superalloys Hardened by γ' and Carbide Precipitation. *Mater. Sci. Eng. A* **2018**, *734*, 437–444. [[CrossRef](#)]
31. Casas, R.; Gálvez, F.; Campos, M. Microstructural Development of Powder Metallurgy Cobalt-Based Superalloys Processed by Field Assisted Sintering Techniques (FAST). *Mater. Sci. Eng. A* **2018**, *724*, 461–468. [[CrossRef](#)]
32. Vajpai, S.K.; Ameyama, K. A Novel Powder Metallurgy Processing Approach to Prepare Fine-Grained Ti-Rich TiAl-Based Alloys from Pre-Alloyed Powders. *Intermetallics* **2013**, *42*, 146–155. [[CrossRef](#)]
33. Sawangrat, C.; Yamaguchi, O.; Vajpai, S.K.; Ameyama, K. Application of Harmonic Structure Design to Biomedical Co-Cr-Mo Alloy for Improved Mechanical Properties. *Mater. Trans.* **2014**, *55*, 99–105. [[CrossRef](#)]
34. Yuan, Y.; Wang, Z.; Zheng, R.; Hao, X.; Ameyama, K.; Ma, C. Effect of Mechanical Alloying and Sintering Process on Microstructure and Mechanical Properties of Al-Ni-Y-Co-La Alloy. *Trans. Nonferrous Met. Soc. China* **2014**, *24*, 2251–2257. [[CrossRef](#)]
35. Vajpai, S.K.; Sawangrat, C.; Yamaguchi, O.; Ciuca, O.P.; Ameyama, K. Effect of Bimodal Harmonic Structure Design on the Deformation Behaviour and Mechanical Properties of Co-Cr-Mo Alloy. *Mater. Sci. Eng. C* **2016**, *58*, 1008–1015. [[CrossRef](#)] [[PubMed](#)]
36. Zhang, Z.; Vajpai, S.K.; Orlov, D.; Ameyama, K. Improvement of Mechanical Properties in SUS304L Steel through the Control of Bimodal Microstructure Characteristics. *Mater. Sci. Eng. A* **2014**, *598*, 106–113. [[CrossRef](#)]
37. Thompson, K.; Lawrence, D.; Larson, D.J.; Olson, J.D.; Kelly, T.F.; Gorman, B. In Situ Site-Specific Specimen Preparation for Atom Probe Tomography. *Ultramicroscopy* **2007**, *107*, 131–139. [[CrossRef](#)]
38. Mughrabi, H. The Importance of Sign and Magnitude of γ/γ' Lattice Misfit in Superalloys—With Special Reference to the New γ' -Hardened Cobalt-Base Superalloys. *Acta Mater.* **2014**, *81*, 21–29. [[CrossRef](#)]
39. Davis, J.R. *ASM Specialty Handbook: Nickel, Cobalt, and Their Alloys*; ASM International: Almere, The Netherlands, 2000; ISBN 978-0-87170-685-0.
40. Li, M.; Coakley, J.; Isheim, D.; Tian, G.; Shollock, B. Influence of the Initial Cooling Rate from γ' Supersolvus Temperatures on Microstructure and Phase Compositions in a Nickel Superalloy. *J. Alloys Compd.* **2018**, *732*, 765–776. [[CrossRef](#)]
41. Mitchell, R.J.; Preuss, M.; Hardy, M.C.; Tin, S. Influence of Composition and Cooling Rate on Constrained and Unconstrained Lattice Parameters in Advanced Polycrystalline Nickel-Base Superalloys. *Mater. Sci. Eng. A* **2006**, *423*, 282–291. [[CrossRef](#)]
42. Singh, A.R.P.; Nag, S.; Chattopadhyay, S.; Ren, Y.; Tiley, J.; Viswanathan, G.B.; Fraser, H.L.; Banerjee, R. Mechanisms Related to Different Generations of γ' Precipitation during Continuous Cooling of a Nickel Base Superalloy. *Acta Mater.* **2013**, *61*, 280–293. [[CrossRef](#)]

Disclaimer/Publisher's Note: The statements, opinions and data contained in all publications are solely those of the individual author(s) and contributor(s) and not of MDPI and/or the editor(s). MDPI and/or the editor(s) disclaim responsibility for any injury to people or property resulting from any ideas, methods, instructions or products referred to in the content.